

# Hydrodynamics between Africa and Antarctica during Austral Summer of 2008 and 2009: Results of the IPY Project

Alvarinho J. Luis, S. M. Pednekar

National Centre for Antarctic and Ocean Research (NCAOR), Earth System Science Organization,  
Ministry of Earth Sciences, Government of India, New Delhi, India  
Email: [alvluis@ncaor.org](mailto:alvluis@ncaor.org)

Received October 23, 2012; revised December 18, 2012; accepted January 12, 2013

## ABSTRACT

A hydrographic section between Cape Town, South Africa and India Bay, Antarctica was sampled by deploying expendable CTD probes during the austral summer of 2008 and 2009. In 2009, the Agulhas Retroflexion (AR) Front was displaced southward by  $1.5^\circ$  latitude, while the northern and southern Polar Front meandered southward by  $1^\circ$  and  $1.4^\circ$  latitude, respectively, relative to their positions in 2008. Geostrophic transport, relative to 1000 m, indicates that Antarctic Circumpolar Current (ACC) flow decreased by 2.5 Sv in 2009 compared to that in 2008. The anticyclones which are detached from the AR facilitates a transport to the southeast Atlantic Ocean ranging between 8 and 12 Sv. Nearly 50% of the ACC transport is confined to the 100 - 500 m layer. A comparison of water mass distribution for 2008 and 2009 suggests that Mode Water distribution was restricted to  $42.5^\circ\text{S}$  and  $41.9^\circ\text{S}$ , and the Antarctic Surface Water extended to  $57.6^\circ\text{S}$  and  $46.6^\circ\text{S}$ , respectively. In 2009, the along track Heat Content (HC) and Salt Content (SC) for the upper 750 m of the water column decreased each by 1% compared to those in 2008. In the ACC domain, the HC and SC dip by 36% and 40% in 2009, respectively. The HC and SC associated with Agulhas Retroflexion Front increase in 2009 by 1% and 2%, respectively, due to an enhanced Agulhas transport of warm and saline water from the tropics by 2%.

**Keywords:** Component; Formatting; Style; Styling; Insert

## 1. Introduction

The ocean region between Africa and Antarctica is characterized by three regimes: the subtropical region to the north of  $40^\circ\text{S}$  -  $42^\circ\text{S}$ ; the circumpolar region between  $40^\circ\text{S}$  -  $42^\circ\text{S}$  and  $55^\circ\text{S}$  -  $57^\circ\text{S}$ , embedded with fronts of the Antarctic Circumpolar Current (ACC); and the eastern limb of the Weddell Sea gyre. Within the subtropical region, the Agulhas Current (AC) constitutes the western limb of the Subtropical gyre of the South Indian Ocean (IO). South of Africa, the AC curls back upon itself and flows into the South IO as the Agulhas Return Current (ARC) along the Subtropical Convergence and continues to flow eastward as the South Indian Ocean Current [1]. After the Agulhas Retroflexion (AR), the AC facilitates a transport of Indian Ocean Central Water of 10 Sv ( $1 \text{ Sv} = 10^6 \text{ m}^3 \cdot \text{s}^{-1}$ ) to the Atlantic, which is a key link to the global thermohaline circulation [2-4]. In the global conveyor system, the Subtropical IO also exports Antarctic Bottom Water (AABW) and diluted North Atlantic Deep Water (NADW) at the deeper depths to the Atlantic Ocean. Down south, the eastward flowing ACC accomplishes an inter-ocean exchange of colder water with

Atlantic, Indian and Pacific Oceans. The hydrological frontal zone in the south IO plays a significant role as a source for atmospheric  $\text{CO}_2$  during austral summer, which contrasts with the majority of the regions which represents  $\text{CO}_2$  sink [5]. Knowledge of the ocean fronts is thus important in determining the atmospheric  $\text{CO}_2$  balance of the region, primary productivity, water mass distributions, circulation, etc. Further south, the Weddell Sea circulation exhibits a cyclonic pattern, with the western limb having higher transport than the eastern counterpart by  $\sim 5 \text{ Sv}$  [6]. The circulation enables transfer of heat and salt from ACC to the Antarctic continental shelves, where deep and bottom waters are formed [7].

The study of southwestern IO is important because of various reasons related to oceanographic and meteorological features. Among the world oceans, about 67% of the total water volume with a temperature from  $-2^\circ\text{C}$  and  $2^\circ\text{C}$  is found in the southwest IO which lies in immediately downstream of the Weddell Sea, where most of this water is formed [8]. The region exchanges a large amount of heat with the atmosphere, and it receives this heat largely from the warm ( $16^\circ\text{C}$  -  $26^\circ\text{C}$ ) and saline AC

water (35.5 psu) which gets trapped in the AR. The south Indian subtropical gyre is unique in that most of the water recirculates in the western and central parts basin [9]. The warming of the Southern Ocean (SO) in the mid-latitude over the past decades [10], due to the austral summertime strengthening of the circumpolar westerlies and weakening of the mid-latitude westerlies from stratosphere to the surface, have forced the southward shift and spin-up of the subtropical gyres [11], thereby advecting more warm water and increasing the ocean heat content southward [12]. The merging of fronts is particularly dramatic in the southwest Indian Ocean, where the Subantarctic Front (SAF) and Polar Front (PF) of the ACC and the Subtropical Front (STF) and ARC are all in close proximity and together produce some of the largest temperature and salinity gradients in the world Ocean [13-15].

Under the project “Monitoring of the Upper Ocean Circulation, Transport and Water Masses between Africa and Antarctica,” the authors deploy expendable conductivity-temperature-depth (XCTD) along the ship track: Cape Town—Prydz Bay—India Bay—Cape Town during austral summer, by taking advantage of the ice-class ships chartered under the Indian Scientific Expedition to Antarctica. The analysis of the XCTD data [16] collected along Cape Town—India Bay (Section-1) and Cape Town—Prydz Bay (Section-2) during the first week of January and mid-March 2008, respectively, indicate that the STF, SAF and PF exhibited double frontal structures, whose meridional meandering is governed by bottom topography through planetary vorticity. We compared the frontal position relative to that of [14,17]. The southern PF (PF1) exhibited a southward shift in its position by 3.5° latitude on Section-1. A northward meander of the southern STF (SSTF) and the northern and southern SAF (SAF1 and SAF2) by 2° - 3.5° and their near-merger facilitated an enhanced baroclinic transport of 12 Sv in the upper 1000 m, just north of Crozet Island. Three anticyclones that detached from the AR were effective in transporting 17 Sv into the southeast Atlantic. The baroclinic transport contributed by the AC and its retroflexion across Section-2 amounted to 17.6 Sv. These results, along with the inferences from the literature, suggest that the ACC and its fronts undergo temporal and spatial variability, both in horizontal and vertical domains; so there is a need to compare year-to-year hydrodynamics.

The aims of this study are to compare 1) the positions of the hydrological fronts; 2) the spatiotemporal variability of the geostrophic transport associated with the individual fronts; and 3) the net baroclinic transport across the quasi-meridional hydrographic section occupied during 2008 and 2009. We also compare geostrophic transport with that estimated from satellite and identify the water masses and compare their zonal extent during aus-

tral summer of 2008 and 2009, along a near-overlapping ship track from Cape Town to India Bay, Antarctica. The purpose of this case study is to quantify the changes observed in two successive years in terms of spatial front meandering, heat and salt content, geostrophic transport, etc., which would serve as benchmark for future studies. The results of this work cannot be extrapolated to infer interannual variability. Though hydrodynamics are compared along a section occupied in January 2008 and March 2009, we assume that the thermohaline changes are negligible between January and March. In fact, other researchers have compared year-to-year frontal dynamics within a season (summer or winter) irrespective of months of the season [14,17].

## 2. Data and Methods

Vertical profiles of temperature and salinity in the upper 1 km of the ocean were recorded by deploying XCTD probes (type: XCTD-3; temperature/conductivity precision:  $\pm 0.02^\circ\text{C}/\pm 0.03 \text{ mS}\cdot\text{cm}^{-1}$ ; depth accuracy:  $\pm 2\%$  of the depth) along the ship track (Figure 1). The hydrographic stations were spaced roughly 30 - 32 nautical miles apart. The section from south of Cape Town ( $34.62^\circ\text{S}$ ,  $18.15^\circ\text{E}$ ) to India Bay, Antarctica ( $69^\circ\text{S}$ ,

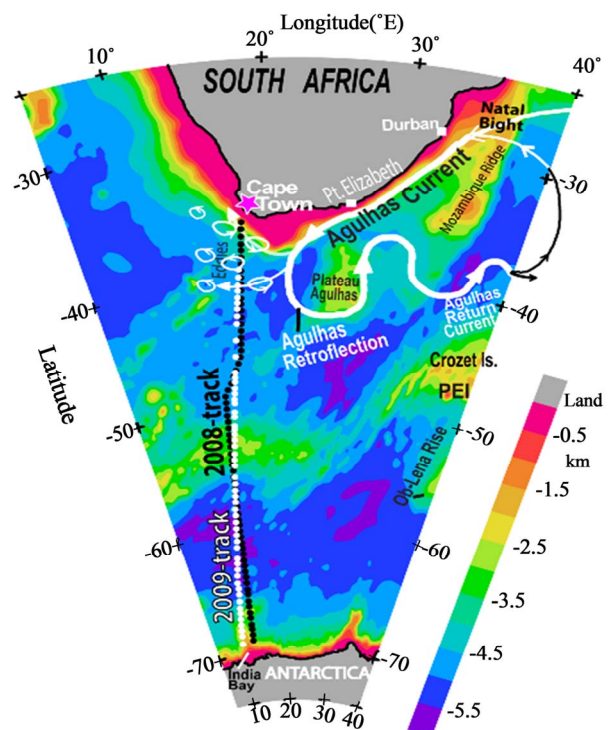


**Figure 1.** Map of the study area overlaid with the positions of the XCTD stations. The stations from the 2008 (2009) survey are shown as black (white) bullets. The bathymetry following [64] is shown in the background, and the schematic of the circulation of Agulhas Current System is superimposed. PEI: Prince Edward Island.

12.97°E) was surveyed during the first week of January 2008 (**Figure 1**, black closed circles) and re-occupied in the third week of March 2009 (**Figure 1**, white closed circles). We did not apply fall rate correction because a comparison of XCTD-3 and Sea Bird CTD profiles revealed that the former is consistent with temperature and salinity accuracy specified by the manufacturer [18], and the fall rate for XCTD showed no systematic bias in the fall rate equation provided by the manufacturer [19]. The temperature profiles were quality controlled by following the standard [20]; the reader is referred to [16] for complete details. High frequency noise in the salinity profiles was mitigated by applying a median filter with a 15-m window [21].

We used ocean temperature and salinity as criteria to identify the locations of fronts since these properties can vary as a result of gradual modification of the adjacent water masses by air-sea interaction and cross-frontal mixing [14]. We located the central position of the front by using these values at axial locations at a given depth, e.g., temperature at surface ( $\theta_0$ ) or at 200 m ( $\theta_{200}$ ) and salinity at surface ( $S_0$ ) or at 200 m ( $S_{200}$ ) [22]. Several surface criteria, such as surface temperature and its gradient [23] and surface salinity have been proposed to identify frontal structures, but these can vary with seasons and geographical location. The temperature and salinity criteria employed to identify fronts and water masses is summarized elsewhere [16]. The geostrophic transport ( $T_{sv}$ ) across a pair of XCTD stations was estimated, relative to the deepest common level (1000 db), by using:

$$T_{sv} = \frac{1}{f} \int_{-1000}^0 \Delta\Phi dz,$$

where  $f$  is the Coriolis parameter ( $s^{-1}$ ) at a mean latitude,  $dz$  is the depth interval (m) and  $\Delta\Phi$  is the geopotential anomaly ( $m^2 \cdot s^{-2}$ ) between an adjacent station pair.

We also used the “Maps of Absolute Dynamic Topography (MADT)” with  $1/3^\circ \times 1/3^\circ$  resolution produced by merging TOPEX/Poseidon, JASON-1, ERS-1/2 and Envisat altimeters [24]. The MADT is the sum of the sea level anomaly data and a mean dynamic topography (Rio05-Combined Mean Dynamic Topography (CMDT)). The CMDT is a combined product using the *in-situ* measurements (hydrographic and surface drifter data), altimetry data and the EIGEN-GRACE 03S Geoid. The CMDT is computed over a seven year period (1993-1999). Since the ACC is characterized by fine-scale structures and variability, we used “up-to-date” absolute dynamic topography data and absolute geostrophic velocity components. The details on the mapping methods and different corrections applied to these fields are available elsewhere [25]. Using the altimetry-based geostrophic velocity

components, sea surface convergence  $\left(\frac{\partial u}{\partial x} + \frac{\partial v}{\partial y}\right)$  was

computed to infer upwelling and downwelling signatures in the thermohaline structures. Surface convergence (divergence) indicates downwelling (upwelling). An examination of the vertical thermohaline structure suggests that it is inappropriate to assume the level-of-no-motion at 1000 db to estimate volume transport from XCTD data. So, we have also estimated transport, referenced to ocean geoid, from altimeter (MADT) data by using:

$$T_{surf} = \frac{gD}{f} \Delta SSH,$$

where  $g$  is gravity ( $m \cdot s^{-2}$ ),  $D$  is the thickness of the water column (m), and  $\Delta SSH$  is the sea surface height difference (m). It has been demonstrated that  $\Delta SSH$  across the Kuroshio can be used as a proxy for the full depth transport [26]. The geostrophic currents were estimated from MADT using geostrophic relations.

To gain insights into the background conditions that existed during the period of sampling, we used sea surface temperature ( $T_s$ , version 5) derived from the Advanced Microwave Scanning Radiometer (AMSRE) flown on Aqua satellite [27]. The AMSRE instrument scans conically with a swath width of 1450 km at an incidence angle of  $55^\circ$ . It has field-of-views of  $26 \times 16$  km and  $14 \times 10$  km with its 18.7 and 36.5 GHz channels, respectively, due to which the measurements are recorded in consistent cloud cover conditions. The ocean heat content ( $HC$ ,  $J \cdot m^{-2}$ ) for vertical oceanic column was computed by using

$$HC = \rho C_p \left[ \int_0^{750} T dz \right],$$

where  $\rho$  is the seawater density at surface ( $kg \cdot m^{-3}$ ) and  $C_p$  is the specific heat of seawater at constant pressure at surface ( $J \cdot kg^{-1} \cdot K^{-1}$ ),  $dz$  is the thickness of ocean layer with temperature mean  $T$  ( $^\circ K$ ). Similarly, the salt content ( $SC = \int_0^{750} 0.001 \rho S dz$ ,  $kg \cdot m^{-2}$ ) was estimated from salinity profiles (with  $S$  in psu).

## 3. Results and Discussion

### 3.1. Satellite Observations

**Figure 1** shows the topographic features of the study area overlaid with locations of the XCTD stations. The generalized schematic of the AC system superimposed on **Figure 1** was constructed by referring to the MADT and  $T_s$  fields. It observed that the subtropical gyral circulation in the southwestern IO is stronger than that in the other two oceans. It is also noted that the gyre is asym-

metric in nature because the circulation in the western limb is stronger because most of the water recirculates in the western and central parts (up to  $70^{\circ}\text{E}$ ) of the ocean basin [9]. At the AR, the anticyclonic eddies which are detached from the current are carried into the Atlantic Ocean, are effective in promoting an exchange of salt and mass. **Figures 2(a)** and **(b)** depicts the MADT, superimposed with altimetry-based geostrophic currents. The outline of AC, AR and ARC are traced out following the 2.4-dyn contour (**Figures 2(a)** and **(b)**). The AM-SRE-based  $T_s$  maps for 2008 (left panel) and 2009 (right panel) are portrayed on **Figures 2(c)** and **(d)**, where the AC flow can be roughly represented by the  $22^{\circ}\text{C}$  contour

in 2008 and by  $23^{\circ}\text{C}$  in 2009 map. Since the sampling from Cape Town to India Bay was completed in about 10 days, **Figures 2(a)-(d)** represents a 10 day average for the survey period.

In 2008, the AC extends up to  $40^{\circ}\text{S}$ , while its southernmost limit in 2009 is traced to  $39^{\circ}\text{S}$  (**Figures 2(a)** and **(b)**). The AC retroflects onto itself at about  $22.5^{\circ}\text{E}$ ,  $40^{\circ}\text{S}$  in 2008 and at  $24^{\circ}\text{E}$ ,  $39^{\circ}\text{S}$  in 2009, curves northeastwards and continues to flow into the southwest IO as ARC in a convoluted pattern [28] which is dominated by a number of anticyclones. The ARC is characterized by an elevated surface topography ( $\sim 2.7$  dyn m, **Figures 2(a)** and **(b)**). Along the southeast coast, the upwelling-favorable

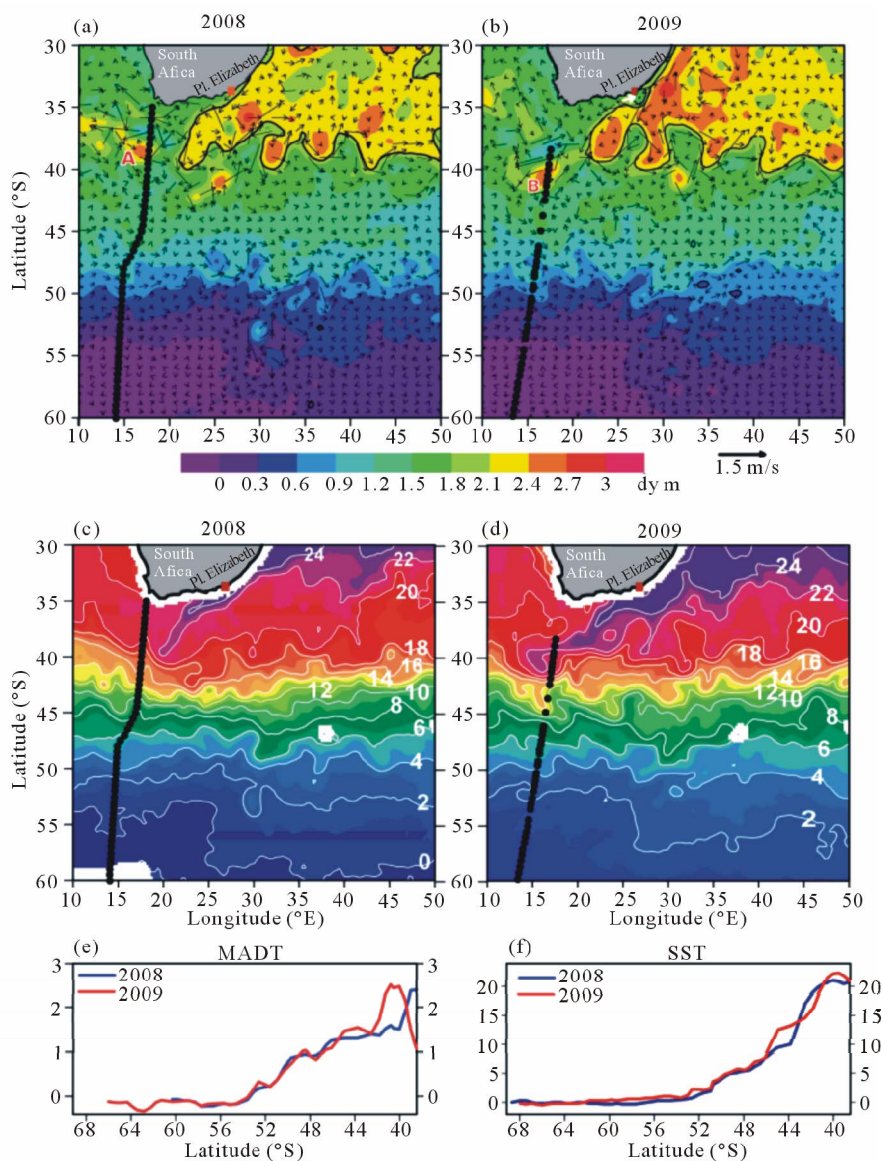


**Figure 2.** (a) and (b) represent absolute dynamic topography overlaid with geostrophic velocity components (displayed at every third grid for clarity); (c) and (d) sea surface temperature ( $^{\circ}\text{C}$ ) field derived from the advanced microwave scanning radiometer onboard NASA's Aqua satellite. The XCTD stations are overlaid as black bullets; (e) MADT; and (f) AM-SRE-based SST for 2008 and 2009 along the track.

wind-stress curl in 2009 promotes a low-SST over a large area depicted by the 24°C contour, which is marked by a relief in dynamic topography (<1.8 dyn m). We note that the isotherms in 2009 representing SST of 22°C to 24°C are displaced southward off the Port Elizabeth due to the Natal Pulse (NP). It is a solitary meander initiated by a baroclinic instability at the Natal Bight (just north of Durban), when the intensity of the landward border of the current exceeds a certain threshold [29] (**Figure 2(d)**). The NP in the Natal Bight area (**Figure 1**) occurs at irregular intervals with a periodicity ranging from 50 to 240 days [30]. The NPs, which are generated at the Natal Bight by anticyclonic eddies (see white arrow pointing to the eddy on **Figure 2(b)**), move downstream along the AC at speeds about 20 km·day<sup>-1</sup> [31] and widen the AC to about 300 km seaward of its usual location. The NP is also known to cause major disruptions to the AC flow, including retroreflections off Port Elizabeth, which inhibits the flow of water to the AR region, thereby providing less water for inter-ocean transfers. A number of warm and cold-core eddies are shed from the AR and ARC due to fluctuations in the Rossby waves on the ARC. During 2008 an anticyclone with a 130-km diameter (represented by letter A) was identified with its core at 17°E, 38.5°S in the MADT map. It is characterized by a dynamic topography of 2.7 dyn·m,  $T_s$  of 20°C - 21°C, and rotational velocity of 1.5 m·s<sup>-1</sup>. In 2009, we detected an oval-shaped anticyclone (represented by letter B) with a diameter of 220 km and oriented in the northeast-southwest direction in the MADT map. Its core is located at 16.3°E, 41°S and it is characterized by surface dynamic topography of 2.7 dyn·m,  $T_s$  of 22°C, and radial velocity of 1.2 m·s<sup>-1</sup>. These eddies spawn across the Subtropical Convergence and are responsible for a substantial meridional heat flux into the SO [32], and their genesis is linked to natural fluctuations in the current or to the adsorption of deepsea eddies into the current. In the climate change scenario, marked by altered wind stress curl over the south IO, it is plausible that the threshold for the triggering of a NP will occur more frequently. A sharp SST gradient in the contours marks the northern extent of the ACC which extends from 42.8°S to 51°S, marked by a SST range of 3°C - 12°C in 2008 and from 43.8°S to 52.8°S with a SST range of 2°C - 9°C in 2009.

South of the continental shelf of South Africa, the AC retroreflects onto itself and curls westwards and flows eastward as the ARC [33]. The occurrence of AR over the western half of the Agulhas Plateau can be explained as follows. Baroclinic flows over smoothly varying topography tend to conserve angular momentum by following lines of constant potential vorticity approximated by  $PV = (f + \zeta)/H$ , where  $f$  is planetary vorticity (s<sup>-1</sup>),  $\zeta$  is relative vorticity (s<sup>-1</sup>), and  $H$  is water depth (m). In open ocean,  $f$  is much larger than  $\zeta$ , so that the mean  $PV$  can be

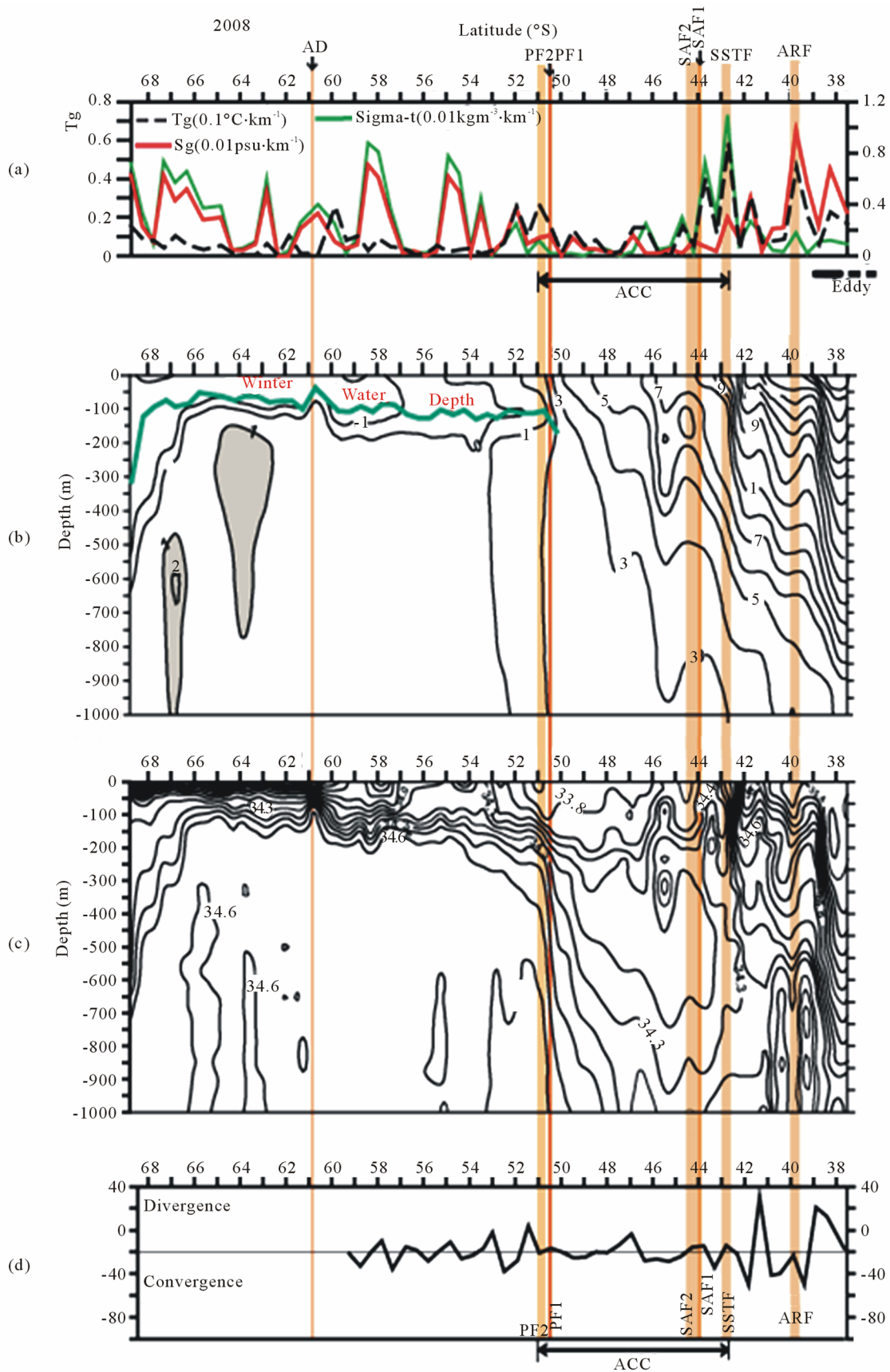
approximated by  $f/H$ . In SO, significant changes in the depth associated with mid-oceanic ridges and uneven bottom topography cause the ACC jets to deviate from the circumpolar lines of constant PV [34]. Having encountered a sharp gradient in the bottom topography (from ~500 m over the Agulhas Bank to ~5000 m, **Figure 1**), the AC progrades into the South Atlantic Ocean and retroreflects back on itself. Here the exchange of Agulhas water between the South IO and South Atlantic Ocean is facilitated by Agulhas rings and to a lesser extent by Agulhas filaments [35]; the remainder of the AC water flows eastward in a series of steady state meanders of 700-km wavelength and amplitudes that decrease from 170 km in the first meander to 50 km in the following meanders. The vorticity balance of the meandering ARC speed axis has been analysed elsewhere [36] and it has been demonstrated that the balance between the beta term (meridional gradient of Coriolis force) and advection of curvature vorticity makes the ARC axis horizontally non-divergent.

We note that the AR region is associated with a very high eddy kinetic energy (EKE) [37], which makes it a “Cape Cauldron” characterized by turbulent stirring and mixing promoted at surface and intermediate depths [28], [29]. They demonstrated that the enhanced EKE field is for the most part composed of surface-intensified cyclonic and anticyclonic vortices from both the Indian and the Atlantic Oceans.

We compare the variability in MADT and SST (for 2008 and 2009) referring to **Figures 2(e)** and **(f)**, respectively. North of 45°S, the difference in MADT for 2009 is found to be higher than for 2008, which is due to the fact that the eddy was further north in 2008 and the observations were stopped due to technical reasons at about 38°S, so the signature of the whole eddy is not captured. It is noted that the SST variation in 2009 is higher due to the presence of filaments of warm water (15°C) protruding southward to ~45°S (**Figure 2(d)**). With the background knowledge of these surface manifestations inferred from satellite observations, the features identified from the vertical temperature and salinity sections are discussed in the next subsection.

### 3.2. Hydrological Fronts and Thermohaline Characteristics

**Figure 3** depicts surface gradients of  $T_s$ ,  $S$  and  $\sigma_t$  along with vertical distributions of XCTD-based temperature and salinity along the ship track. Surface convergence inferred from altimeter-based absolute geostrophic velocity components were used as guide in the interpretation of the changes and the nature of eddies reflected in the thermohaline structure (**Figures 3(d)** and **(h)**). We used temperature and salinity as criteria for identification of



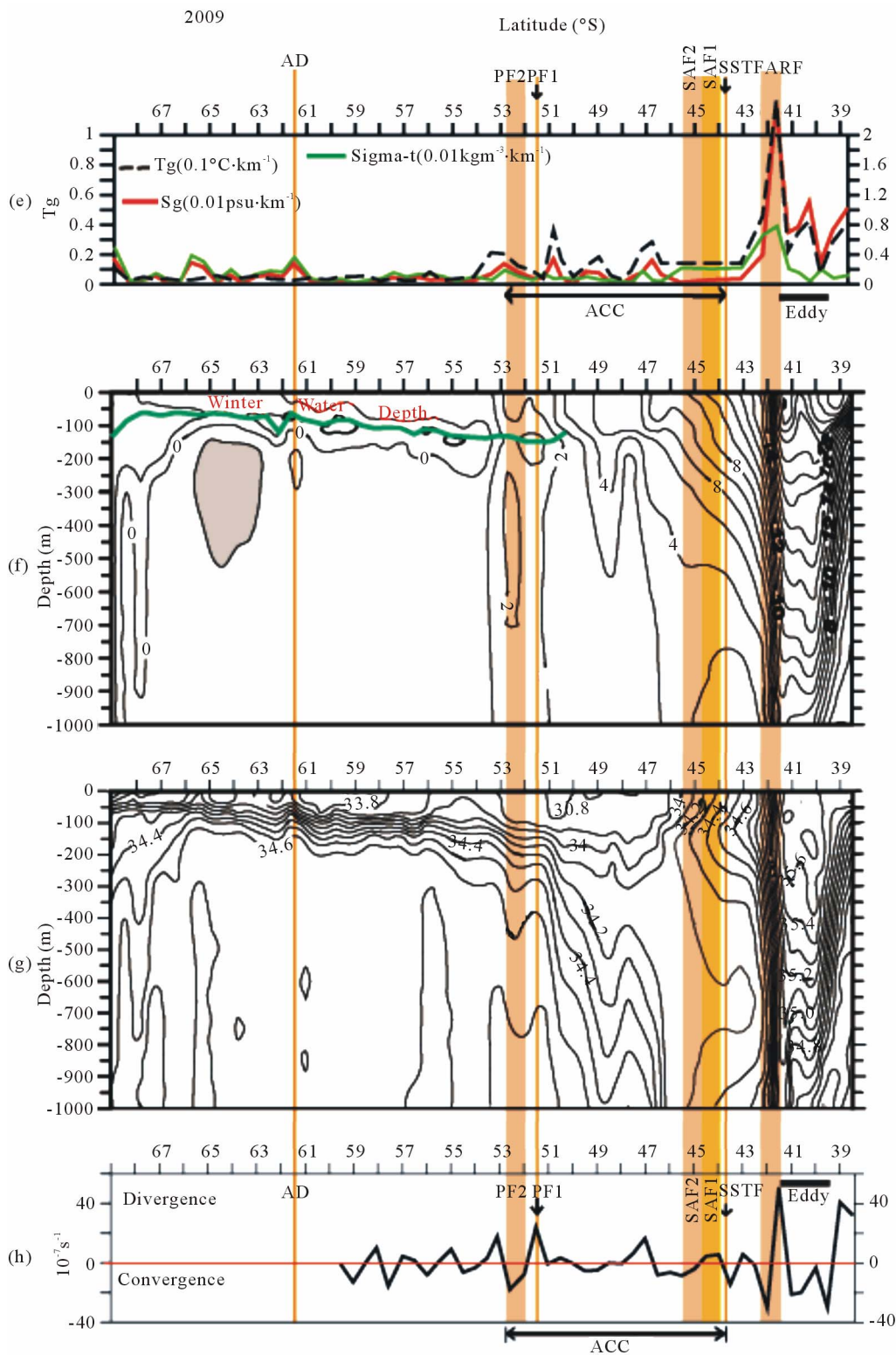


**Figure 3.** (a) Absolute gradient of temperature (Tg), salinity (S) and sigmat at surface; Vertical section of (b) temperature ( $^\circ\text{C}$ ); (c) Salinity (psu); and (d) sea surface divergence from satellite-based surface depicted on panel 3b. The distribution of hydrological fronts are also shown. The distribution of the hydrological fronts is shown by vertical lines. The abbreviations are: ARF: Agulhas Retroreflection Front; SSTF: Southern Subtropical Front; SAF1 and SAF2: northern and southern Subantarctic Front; PF1 and PF2: northern and southern Polar Front; and AD: Antarctic Divergence, and ACC: Antarctic Circumpolar Current. Same as in Figure 3(a)-(d), but for 2009. The winter water depth is depicted on panel 3f.

the locations of hydrographic fronts following our earlier work [16]. In this work, the ACC extends from the SSTF in the north to the southern limit of the PF2.

The ARF in 2008 extends from 39.8°S to 40°S (**Figure 3(a)-(c)**). It is marked by gradients of  $T_s$ ,  $S$  and  $\sigma_t$ , of  $4.5 \times 10^{-1} \text{ }^\circ\text{C}\cdot\text{km}^{-2}$ ,  $9 \times 10^{-3} \text{ psu}\cdot\text{km}^{-1}$  and  $1.5 \times 10^{-3} \text{ kg}\cdot\text{m}^{-3}\cdot\text{km}^{-1}$ , respectively (**Figure 3(a)**). The surface convergence of  $3 \times 10^{-7} \text{ s}^{-1}$  (**Figure 3(d)**) corresponds to a wedge-shaped structure in the upper 200 m in the vertical temperature and salinity structure at the ARF (**Figures 3(e) and (d)**). In 2009, the ARF exhibits gradients of  $T_s$ ,  $S$  and  $\sigma_t$ , of  $1.2 \times 10^{-1} \text{ }^\circ\text{C}\cdot\text{km}^{-1}$ ,  $24 \times 10^{-3} \text{ psu}\cdot\text{km}^{-1}$  and  $6.5 \times 10^{-3} \text{ kg}\cdot\text{m}^{-3}\cdot\text{km}^{-1}$ , respectively (**Figure 3(e)**). The surface divergence ( $6 \times 10^{-7} \text{ s}^{-1}$ , **Figure 3(h)**) in ARF domain (41.5°S - 42.3°S) reflects the sharp vertical gradients promoted by upwelling at the southern periphery of an anticyclonic eddy (**Figure 2(c)**) in the thermohaline structure (**Figure 3(f) and (g)**). Moving southward, the southern STF (SSTF) in 2008 is traced between 42.8°S and 43°S, which is characterized by the  $T_s$ ,  $S$ , and  $\sigma_t$  gradient of  $5.7 \times 10^{-2} \text{ }^\circ\text{C}\cdot\text{km}^{-1}$ ,  $9 \times 10^{-3} \text{ psu}\cdot\text{km}^{-1}$  and  $2.5 \times 10^{-3} \text{ kg}\cdot\text{m}^{-3}\cdot\text{km}^{-1}$ , respectively (**Figure 3(a)**). The surface divergence ( $5 \times 10^{-7} \text{ s}^{-1}$ , **Figure 3(d)**) at SSTF corresponds to the upwelling scenario revealed from the thermohaline structure (**Figures 3(b) and (c)**). In 2009, the SSTF is located at 43.8 is marked by weak  $T_s$ ,  $S$  and  $\sigma_t$  signatures which corresponds to surface convergence ( $7 \times 10^{-7} \text{ s}^{-1}$ , **Figure 3(h)**). The SSTF, which forms a boundary between subtropical and Antarctic water, is marked by subsurface intrusion of high salinity water in the upper 250 m southward (**Figure 3(f) and (g)**).

The merged northern SAF (SAF1) and southern SAF (SAF2) spans 44°S to 44.7°S and 44 - 45.5 in 2008 and 2009, respectively (**Figures 3(b), (c), (f) and (g)**). Compared to SAF2, SAF1 in 2008 is marked by strong  $T_s$ ,  $S$  and  $\sigma_t$  signatures of  $4 \times 10^{-2} \text{ }^\circ\text{C}\cdot\text{km}^{-1}$ ,  $5 \times 10^{-3} \text{ psu}\cdot\text{km}^{-1}$  and  $10 \times 10^{-3} \text{ kg}\cdot\text{m}^{-3}\cdot\text{km}^{-1}$ , respectively (**Figure 3(a)**). The surface divergence ( $3 \times 10^{-7} \text{ s}^{-1}$ , **Figure 3(d)**) at the merged front reveals weak upwelling signatures in the thermohaline structure (**Figures 3(b) and (c)**). The surface gradients in  $T_s$ ,  $S$  and  $\sigma_t$  appear weak, and upwelling signatures are revealed in vertical structures in 2009 (**Figures 3(f) and (g)**). It is pertinent to note that [38] identified a merged front (SSTF+SAF1+ARF) between 40.3°S and 43°S by using CTD data along 45°E section. Similar concatenation of these three fonts was reported elsewhere by using satellite-based multichannel sea surface temperature [23].

The PF, which acts as a boundary between the Agulhas Basin to the north and the Enderby Basin to the south, splits into the northern PF1 and southern PF2. Based on  $T_{\min}$  layer at 200 m and the northernmost extent of 2°C below 200 m ([14,39,40]) we traced PF1 to 50.4°S and 51.5°S in 2008 and 2009, respectively. The PF1 is char-

acterized by  $T_s$ ,  $S$  and  $\sigma_t$  of  $1.5 \times 10^{-2} \text{ }^\circ\text{C}\cdot\text{km}^{-1}$ ,  $1.5 \times 10^{-3} \text{ psu}\cdot\text{km}^{-1}$ ,  $0.2 \times 10^{-3} \text{ kg}\cdot\text{m}^{-3}\cdot\text{km}^{-1}$ , respectively (**Figure 3(a)**) in 2008 and corresponding values in 2009 are  $0.8 \times 10^{-2} \text{ }^\circ\text{C}\cdot\text{km}^{-1}$ ,  $1 \times 10^{-3} \text{ psu}\cdot\text{km}^{-1}$ ,  $1 \times 10^{-3} \text{ kg}\cdot\text{m}^{-3}\cdot\text{km}^{-1}$ . Surface divergence of  $2 \times 10^{-7} \text{ s}^{-1}$  and  $20 \times 10^{-7} \text{ s}^{-1}$  in 2008 and 2009, respectively, facilitates strong upwelling signature at PF1. PF2 extended from 50.6°S to 51°S in 2008 which shifts southward and extends from 52°S to 52.8°S in 2009. The PF2 coincides with a region where subsurface (<150 m) intrusion of cold Antarctic water northward is identified (**Figure 3(b), (c), (f) and (g)**); its surface expression is marked by convergence ( $\sim 1 \times 10^{-7} \text{ s}^{-1}$ ) during both years. We note that [22] identified PF1 as a single front at 51°S on the 30°E section, while [38] identified PF1 and PF2 spanning 49°S to 50°S and 52°S to 54°S, respectively, along the 45°E section. The PF2 location proposed by [38] coincided with that of PF in [14]. The branching of PF is attributed to the occurrence of a highly convoluted meander or detached cold and warm eddies [41].

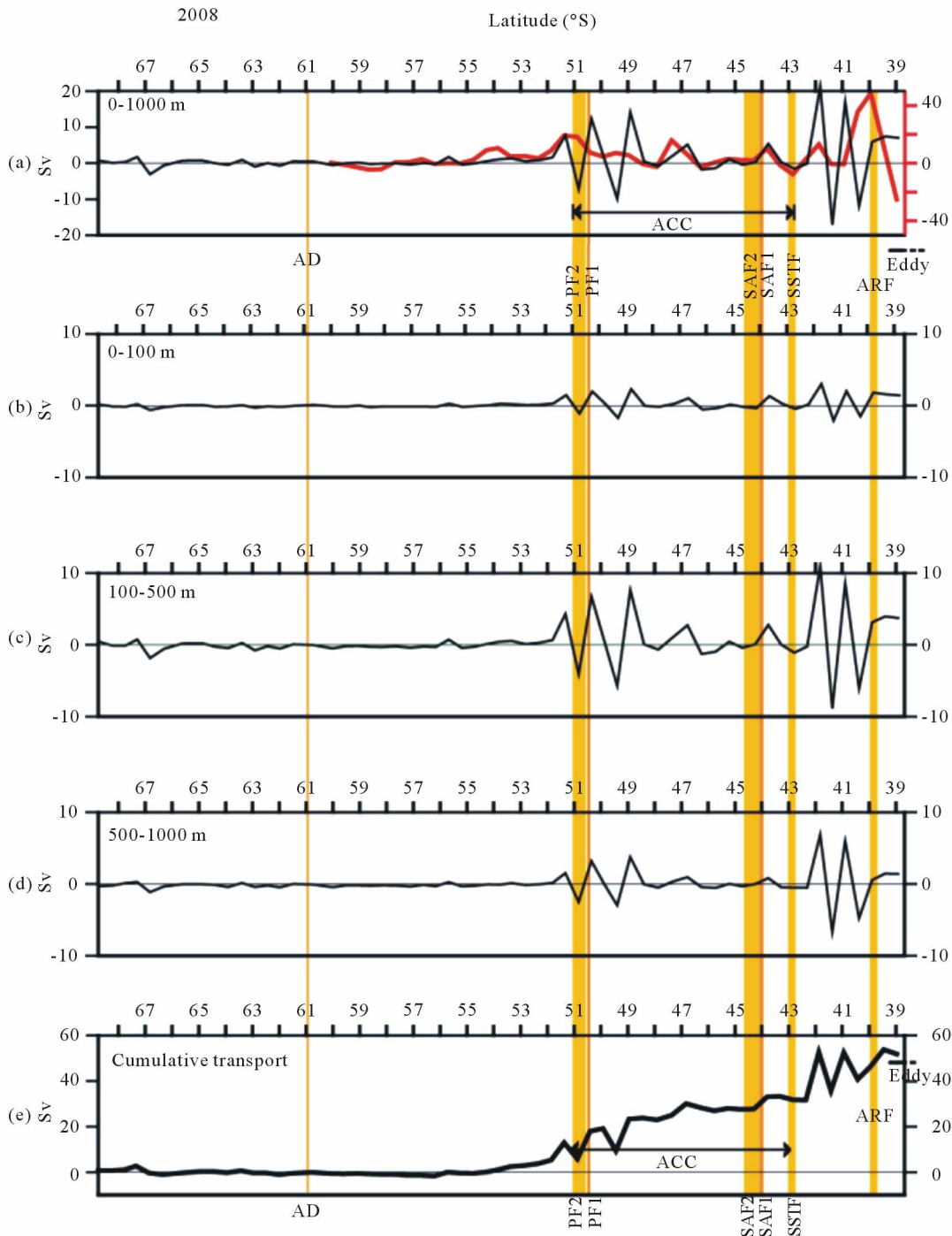
The Antarctic Divergence (AD) is encountered where the shallowest Winter Water (WW) depth was observed. It is characterized by an intense upwelling of Circumpolar Deep Water (CDW, [41]). We identified AD at 60.9°S and 61.5°S in 2008 and 2009, respectively, where the subsurface isolines shoal gradually towards the AD and deepened toward the Antarctic continental margin. At the AD, we encountered weakest  $T_s$  gradient (2 to  $4 \times 10^{-3} \text{ }^\circ\text{C}\cdot\text{km}^{-1}$ ), but enhanced gradients of  $S$  ( $2.5 \times 10^{-3} \text{ psu}\cdot\text{km}^{-1}$ ) and  $\sigma_t$  ( $3.8 \times 10^{-3} \text{ kg}\cdot\text{m}^{-3}\cdot\text{km}^{-1}$ ) for both years. It is noted that the subsurface weakening of temperature minimum between 63°S and 66°S in the surveys is related to the upwelling of warmer ( $\sim 1^\circ\text{C}$ ) and saline (34.6 psu) deep water at the AD, concurring with findings in [42]. The melt water forces the high saline and denser water ( $>27.7 \text{ } \sigma_t$ ) to flow to deeper depths. Along the Antarctic continent the WW depth is deepens to 300 m in January 2008 which is reduced to 150 m in March 2009, which is most likely a result of seasonality. In particular, in January 2008 the sea is still governed by sea-ice melting, while in March 2009 the first signs of freezing results in several patches of water colder than  $-1^\circ\text{C}$ , which extends to 54°S.

The general features hydrographic characteristics can be summarized as follows. The 2008 track passed over anticyclone centered on at 17°E, 38.5°S, which was characterized by a surface topography of 2.7 dyn m,  $T_s$  of 20°C - 21°C and  $S$  of 35.5 psu. The eddy had a diameter of  $\sim 130$  km and it exhibited a bowl-shaped pattern in the thermohaline structure (**Figures 3(b) and (c)**). In 2009, we detected an anticyclone with a diameter of 220 km along northeast-southwest direction, centered on 16.3°E, 41°S (**Figure 2(b)**). It was characterized by a surface dynamic topography of 2.7 dyn m (**Figure 2(b)**) and  $T_s$  of 22°C (**Figure 2(d)**). The eddy was characterized by a

bowl-shaped in the vertical thermohaline structures (**Figures 3(f) and (g)**). The WW depth varied from 100 m in 2008 to 80 - 90 m (on average) in 2009 (**Figures 3(b) and (f)**). In the Antarctic zone, the cold tongue characterized by  $-1^{\circ}\text{C}$  contour, protruded northward to  $57.3^{\circ}\text{S}$  and  $65.5^{\circ}\text{S}$  in 2008 and 2009, respectively. The most conspicuous feature observed in the vertical structure is the southward shift of the fronts associated with the ACC fronts in 2009.

### 3.3. Baroclinic Transport

**Figure 4** portrays the baroclinic transport, referenced to the deepest common level of 1000 db, across the track for different depth layers: (a) & (f): 0 - 1000 m, (b) & (g): 0 - 100 m, (c) & (h) 100 - 500 m, and (d) & (e) 500 - 1000 m. The zonal extent of the hydrological fronts is also shown. The full-depth altimeter-based transport is depicted in red on panel **Figure 4(a) and (f)** for 2008



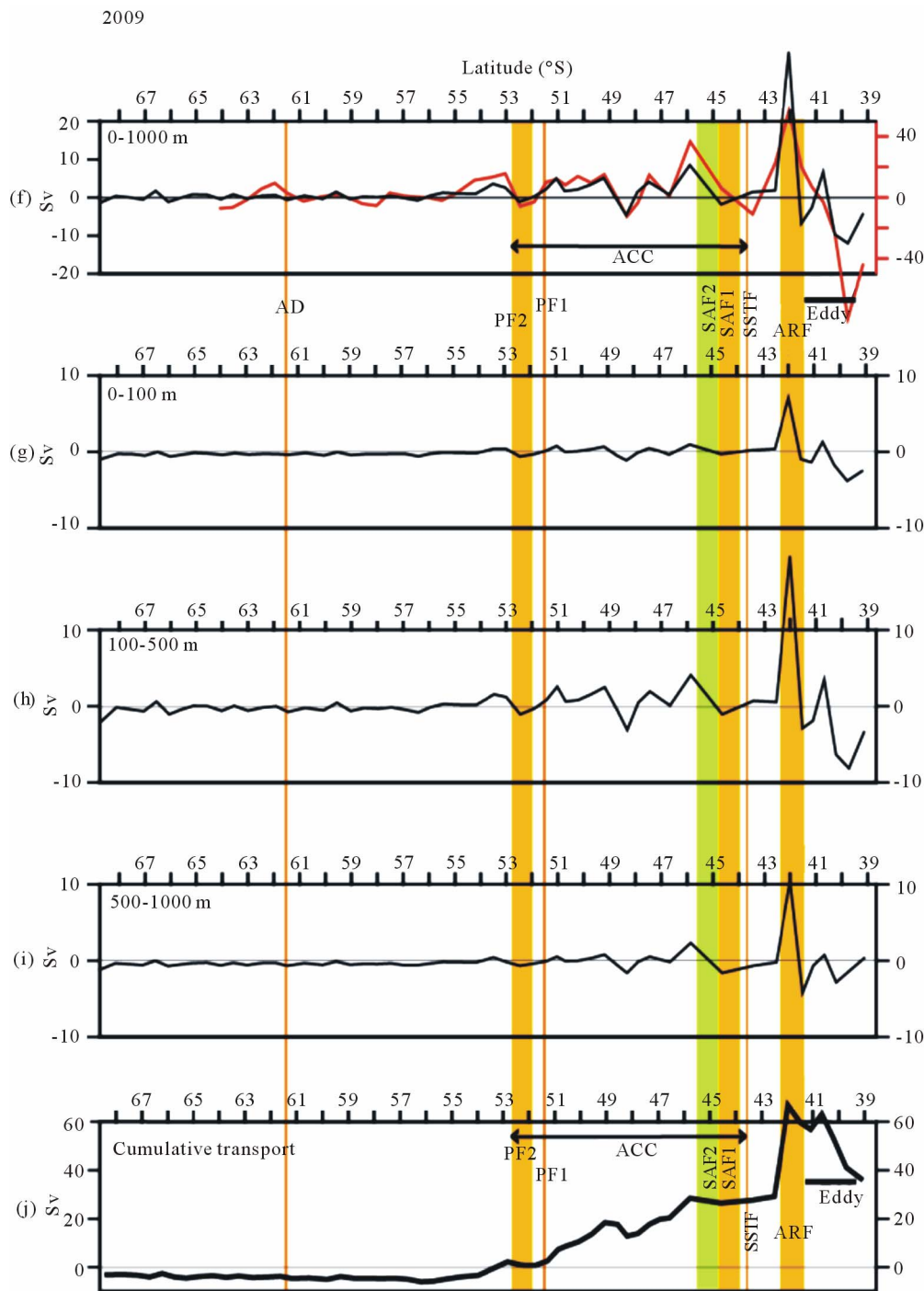


**Figure 4. Geostrophic transport ( $1 \text{ Sv} = 10^6 \text{ m}^3 \cdot \text{s}^{-1}$ ) relative to the 1000 m estimated between a pair of XCTD stations for depth layers: (a) 0 - 1000 m; (b) 0 - 100 m; (c) 100 - 500 m; (d) 500 - 1000 m; and (e) cumulative transport, for 2008. Eastward transport is positive. Geostrophic transport for 2009.**

and 2009, respectively. For the transport computations we involved the XCTD station from  $38.6^\circ\text{S}$  to  $68.5^\circ\text{S}$ . Negative values of transport indicate flow towards west. The net transport in the upper 1000 m across the 2008 track was 61 Sv, which represented  $\sim 66\%$  of the transport estimated, relative to 2500 db, across a section from

Good Hope to Antarctica ( $90 \pm 2.4 \text{ Sv}$ ; Swart *et al.*, 2008). Our value represents 57% of the full depth transport (107 Sv) estimated from altimeter data (red line on **Figure 4(a)**). The jets associated with SAF1, SAF2, and PF1 transported 4, 0.1, 10 Sv, respectively, in 0 - 1000 m layer. Westward directed jets associated with SSTF and

PF27 were effective in a transport of 2 Sv and 7 Sv, respectively. The transport associated with ACC in 2008 was 29.5 Sv, of which 17 Sv was confined to 100 - 500 m layer. The jets associated with the rest of the fronts were effective in transporting slightly more than 50% of the flow in the 100 - 500 m layer.

For the 2009 transect (**Figure 4(f-j)**), we estimated a net eastward transport of 38 Sv, of which 27 Sv were associated with ACC, 39 Sv with ARF, 1 Sv with SSTF, 2 Sv with SAF1, 4 Sv each with SAF2 and PF1. It is pertinent to note that the mean baroclinic transport relative to 2500 db estimated in the literature across sections occupied near the Greenwich Meridian ranges from 87.5 to 109.6 Sv ([43,44]). It is again noted that about 57% of ACC transport (15.5 Sv) occurs in the 100 - 500 m layer.

The transport associated with the leakage at the AR promoted by eddy in 2008 and 2009 amounts to 8 and 12 Sv, respectively. We note that [45] estimated a transport to Atlantic of 15 Sv, while [46] provided an estimate of 11 Sv by using the Southern Africa Experiment (SAfE) Regional Oceanic Model system. It has been reported that on average six Agulhas eddies leak 3 to 9 Sv into the Benguela Current and South Equatorial Current each year [47]; our estimates are close to these values. The occurrence of westward transport associated with PF2 (7 Sv in 2008 and 2 Sv in 2009) is due to the meridional meandering of the jets which is induced for PV conservation. PF2 is located over the southwest Indian ridge, so there is a difference of 1500 m in water depth between the location of PF1 and PF2.

In brief, geostrophic transport showed a decrease in the ACC transport by 2.5 Sv in 2009. The southward shift of the frontal positions in 2009 relative to those in 2008 track is evident. The transport associated with the anticyclone that detached from the ARC varied between 8 and 12 Sv. The ACC transport exceeding 50% was confined to 100 - 500 m layer. This can be explained as follows. First, the strong westerly winds impart momentum down to about a kilometer of the upper ocean and maintains the strength of eastward flowing ACC. The Coriolis force facilitates the Ekman transport in the upper 100 - 150 m towards north. Second, most of the SO is stably stratified which facilitates the decoupling of the different density layers thereby, enhancing the horizontal velocity and consequently the zonal volume transport.

### 3.4. Water Masses

**Figure 5** portrays  $\theta - S$  diagrams for stations sampled in 2008 (left-hand panel) and 2009 (right-hand panel). The water masses were identified using the  $\theta - S$  criteria given in our earlier work [16], which was adopted from literature. The spatial distribution and characteristics of the individual water masses are discussed below.

A mixture of water originating from the southwest IO anticyclonic gyre [48] and Mozambique Channel [49] constitutes the Tropical Surface Water (TSW) which is warm ( $\theta$ : 16° - 28°C) and saline ( $S$ : >35.1 psu). The TSW is transported by the AC into the retroflexion region, where it characterized by  $\sigma_t < 27.5$  and occupies depth

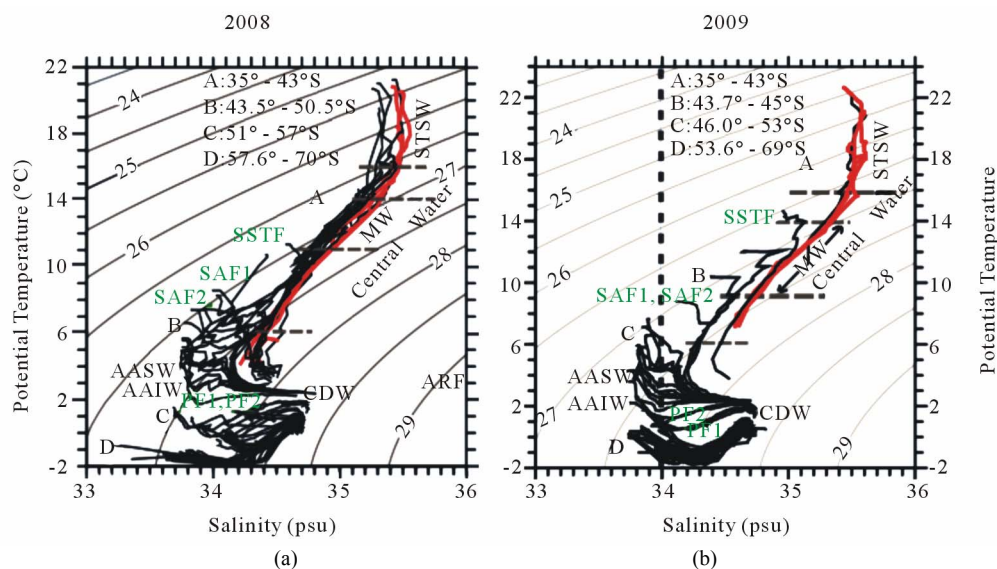


**Figure 5.** The  $\theta - S$  diagram for (a) 2008 and (b) 2009. The  $\sigma_t$  contours ( $\text{kg} \cdot \text{m}^{-3}$ ) are overlaid and the locations of the profiles are shown in clusters (A, B, C, D). The profiles in red are located in the anticyclone that pinched off from the Agulhas Retroflexion. Abbreviations are: TSW: Tropical Surface Water; STSW: Subtropical Surface Water; MW: Subtropical Mode Water; CW: Central Water; SASW: Subantarctic Surface Water; AAIW: Antarctic Intermediate Water; AASW: Antarctic Surface Water; CDW: Circumpolar Deep Water. The vertical dotted line at 34 psu demarcates the STSW, CW, and MW from Antarctic water masses (SASW, AAIW, and CDW).

shallower than 1500 [48]; here it sinks and spreads throughout the south IO and give rise to a salinity maximum. At greater depths, the water flowing within the Retroflection circulation pattern consists primarily of Atlantic and Circumpolar Deep Water. This STSW is traced to 41.5°S (midway between SSTF and ARF) and 41.3°S in 2008 and 2009, respectively. Traced in the upper 70 m north of 39.5°S, it flows down to ~260 m due to the influence of the anticyclone feature along the 2008 track. Likewise, its vertical distribution in 2009 extends to 360 m in the eddy region. The profiles highlighted in red represents the eddy core, which are characterized by high salinity (>34.4 psu) in the upper 400 m.

The Central Water (CW), which is detected below STSW, is formed at the Subtropical Convergence when the mixed Subtropical and SASW sink and spread northward [50]. The CW in the AR region receives a contribution from the South IO and South Atlantic Ocean. The former is characterized by  $\theta$ : 8°C - 15°C and  $S$ : 34.6 - 35.5 psu, while the latter is characterized by  $\theta$ : 6°C - 16°C and  $S$ : 34.5 - 35.5 psu [51]. The South Atlantic Water enters the South Agulhas region as a blend of thermocline water and Subantarctic Surface Water (SASW) from the south [2,52]; hence, these two water masses have nearly similar  $\theta$  and  $S$  range. Characterized by potential density of  $<27.5 \sigma_t$ , CW was detected up to 43.5°S (at SAF1) and 43.7°S (at SSTF) during 2008 and 2009, respectively (**Figures 5(a)** and **(b)**). Its vertical extent varies between 200 - 300 to 860 - 1000 m in the eddy region. It shallows to 450 and 200 m during 2008 and 2009, respectively.

Wintertime convection in the area just to the north of the ACC (north of 43°S) is believed to be involved in the production of the Subtropical Mode Water (MW;  $\theta$ : 11°C - 14°C,  $S$ : 35 - 35.4 psu, and  $\sigma_t$ : 26.5 to 26.8 - 27.24; [38]), which appears as pycnostad or thermostad below the seasonal pycnocline [39]. It contributes volumetrically to the CW of the South IO subtropical gyre by ventilating the upper portion of the permanent thermocline. There are two types of MW: the Subantarctic Mode Water [53] and Subtropical Mode Water (STMW, [54]); the two MW are separated by the Southern STF [14]. We detected STMW up to the location of SSTF (42.5°S) and ARF (42°S) during 2008 and 2009, respectively. The source of the Subtropical Mode Water is the Crozet Basin, where it is produced locally by frontal mixing east of the Crozet Islands (45°S - 47°S) [55]. A significant change in salinity (**Figure 5**) suggests that strong air-sea interaction is involved in its genesis, and the winter overturning of the Subtropical Water of Agulhas origin could be a possible process [53].

The water masses identified in the ACC region consist of the Antarctic Surface Water (AASW), AAIW, and CDW. The AASW ( $\theta$ : < 5°C,  $S$ : < 34 psu) was encoun-

tered in the upper 80 m northward from Antarctica shelf to 57.6°S and between 47°S to 53°S confined to the upper 240 m in 2008. In 2009, its distribution extended up to 46.6°S from the Antarctic shelf; its depth range deepens from 0 - 100 at 53°S to 120 - 180 m southward of SAF2. The AASW has two components: Summer Surface Water (SSW) and Winter Water (WW). The WW forms a temperature minimum layer below the SSW and is characterized by  $\theta$ : -1.9°C to 1.5°C and  $S$ : 34.2 - 34.5. WW is a remnant of the surface water formed by winter convection [56], which spreads northwards to about 50.5°S during both years by westerly winds. The WW depth shallows from 300 m in 2008 to 150 m in 2009.

The AAIW ( $\theta$ : 2.2°C,  $S$ : 33.87) is formed continuously near the PF at 50°S - 55°S (**Figure 3(b), (c), (f)** and **(g)**), where it sinks and spreads northward [57]. The AAIW, which is detected in the southwest IO in the depth range of 40 - 122 m [58], was traced at 50.5°S and between 50.7°S and 51.5°S in 2008 and 2009, respectively. In the literature, AAIW was identified between 31°S and 41°S spanning 1150 and 1200 m along the 45°E section [38]. The most voluminous water mass in the SO is the CDW ( $\theta$ : 2°C and  $S$ : 34.77) which occurs below the AAIW. It is involved in the formation of all other water masses through vertical and lateral mixing facilitated by winds over the Antarctic slope and shelf regions [59]. The CDW consists of the upper CDW and lower CDW. The former is characterized by an oxygen minimum and nutrient maximum and entrained within the ACC, while the latter exhibits a salinity maximum and is found in the vicinity of the Antarctic continental shelf. Because the terminal depth of the XCTD probes is about a km, it is not possible to discriminate between the lower and upper CDW. However, we encountered traces of CDW in the depth range of 600 - 700 m at 51°S and 50.6°S - 51°S in 2008 and 2009, respectively.

### 3.5. Ocean Heat Content

Explosive cyclones dominated the SO south of 45°S [60]. In the ocean, eddies are principal agents of promoting meridional heat transfer [61]. Moreover, fronts are potential zones for atmosphere-ocean heat transfer. Therefore, we expect changes in the oceanic HC at the frontal zones and at the eddy core. The HC and SC for 2008 and 2009 are shown in **Figure 6**. The HC integrated along the track is lowered by 1% from  $3.32 \times 10^{20}$  in 2008 to  $3.28 \times 10^{20} \text{ J}\cdot\text{m}^{-1}$  in 2009. Likewise, the along track integrated SC is lower by 1% from  $1.03 \times 10^{13}$  in 2008 to  $1.02 \times 10^{13} \text{ kg}\cdot\text{m}^{-1}$  in 2009. The root mean square (RMS) difference between the two years amounts to  $32.4 \times 10^8 \text{ J}\cdot\text{m}^{-2}$  and  $2.8 \text{ kg}\cdot\text{m}^{-2}$  for HC and SC, respectively (gray bars in panels **Figures 6(a)** and **(b)**). In the ACC region, HC and SC decreases by  $9227 \times 10^9 \text{ J}\cdot\text{m}^{-2}$  (36%) and 32

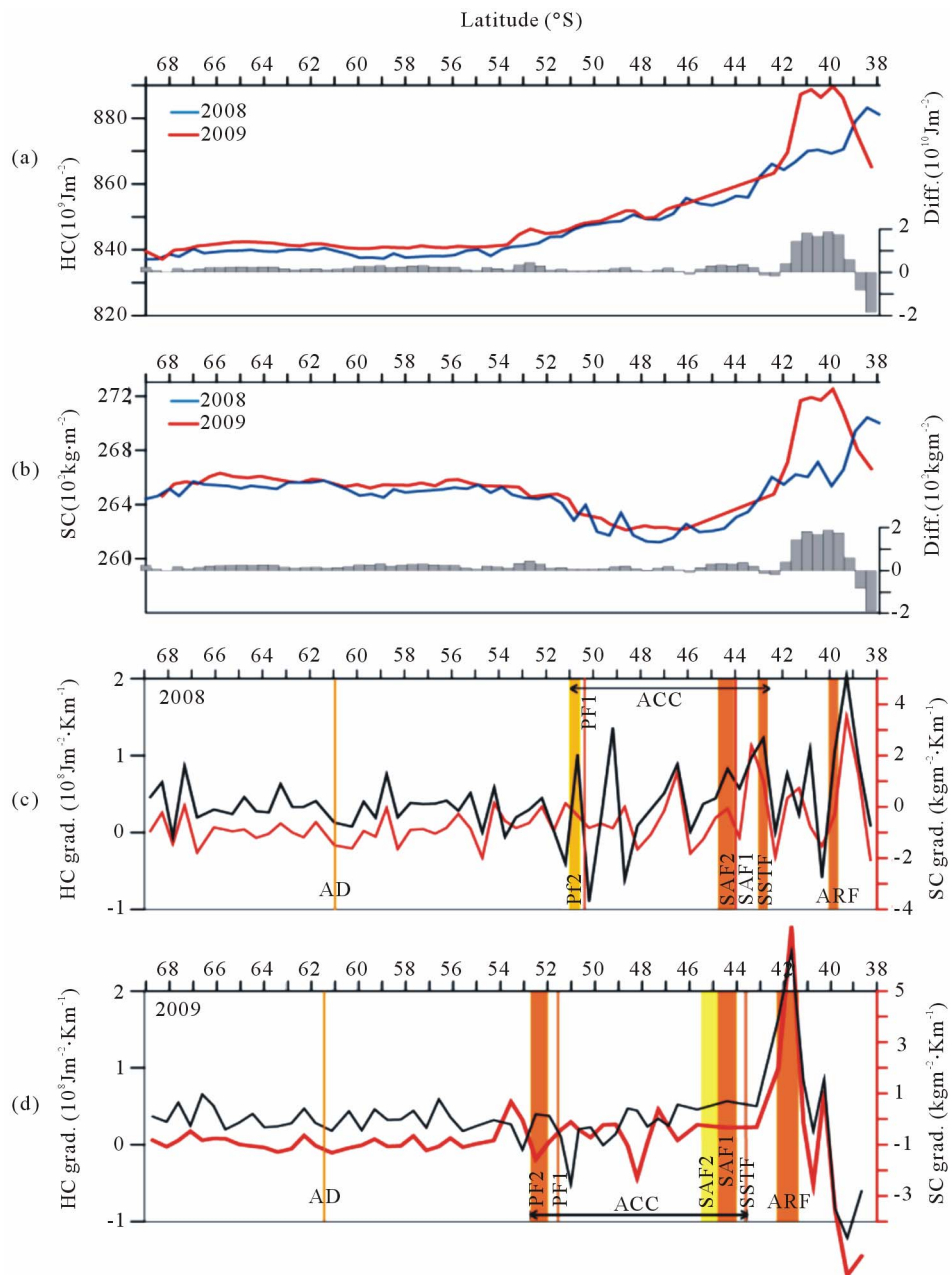


**Figure 6. (a) Heat content (HC) and (b) salt content (SC), for 0 - 700 m layer for 2008 and 2009 XCTD data. The temporal difference (2008-2009) for the HC and SC is shown as gray bars. Along track gradient of HC and SC for (c) 2008 and (d) 2009. The location of the hydrological fronts is highlighted by vertical lines in Figures 6(c) and (d).**

$\times 10^4 \text{ kg} \cdot \text{m}^{-2}$  (40%) in 2009. In 2008, the total HC associated with the merged SSTF + SAF1 + SAF2, PF1 + PF2, and ARF is estimated as  $3429 \times 10^9$ ,  $1690 \times 10^9$  and  $1740 \times 10^9 \text{ J} \cdot \text{m}^{-2}$ , respectively. On the other hand, the HC in 2009 associated with the merged SSTF + SAF1 + SAF2, PF1 + PF2, and ARF amounts to  $2573 \times 10^9$ ,  $2536 \times 10^9$  and  $1757 \times 10^9 \text{ J} \cdot \text{m}^{-2}$ , respectively. The SC associated with SSTF + SAF1 + SAF2 decreases by 25%, but is enhanced by 52% and 2% for PF1 + PF2 and ARF, respectively. The HC and SC associated with the anticy-

clone are estimated to be  $1749 \times 10^9 \text{ J} \cdot \text{m}^{-2}$  and  $5.4 \times 10^4 \text{ kg} \cdot \text{m}^{-2}$  in 2008, which are both increased by 52% in 2009. These large differences arise because the ship track in 2008 passed on the edge of the eddy, while it was centered on the eddy in 2009 (Figure 2(c)). Moreover, the differences are also attributed to a high level of mixing of different water masses associated with the mesoscale turbulence and Indo-Atlantic exchange taking place in this region [4,28,62].

Figures 6(c) and (d) represent the HC and SC gradient

for 2008 and 2009, respectively. Sharp gradients are observed at the ARF and at the periphery of the eddy that pinched off from the ARF (**Figures 2(a) and (c)**). Similarly, pronounced gradients are found in the region of SAF2 + SAF1 + SSTF in 2008 (the same is not clear in 2009 because of large spacing between the stations). It is pertinent to note that along 45°E section, the other researchers observed a sharp change in HC at ~42°S by  $9.8 \times 10^{10} \text{ J}\cdot\text{m}^{-2}$  coinciding with the merged frontal region occupied by ARF + SSTF + SAF1 [38]. The undulation in the HC and SC from 38°S to 40°S indicates the dynamic instability due to the eddy or mesoscale activities related to the exchange of Agulhas water between the South IO and South Atlantic Ocean facilitated mostly by large Agulhas rings and to some extent by Agulhas filaments [35]. PF2 exhibits a slightly higher gradient in HC in 2008, which could be due to a slightly higher baroclinic transport (5 Sv) in the 100 - 500 m layer. The SSTF which is located at the Subtropical Convergence shows a higher degree of HC variability which promotes a faster meridional transport of heat from subtropics to polar region. This suggests that the observed variation of HC and SC influences the meridional heat and salt transfer which is crucial to the regional climatic variability. For example, when the sea surface temperature within the ARF and AC is higher, the summer rainfall over southern regions is higher [63]. The differences in SC and HC were higher north of 48° due to mesoscale turbulence and Indo-Atlantic exchange mediated by eddies.

#### 4. Conclusions

Hydrographic surveys were undertaken during austral summer of 2008 and 2009 from Cape Town to India Bay, Antarctica, by deploying XCTD to obtain a quasi-synoptic picture of the subtropical and ACC frontal structure, water masses and geostrophic transport. To support hydrographic observations, we incorporated satellite-based altimeter and AMSRE-based SST data for 2008 and 2009, which revealed the southern extent of the AC, the presence of Natal Pulse features, and the characteristics patterns of the anticyclones released by AR, which transports warm and salty water to the southeast Atlantic Ocean amounting to 8 and 12 Sv in 2008 and 2009, respectively. This leakage contributes to the upper limb of the Atlantic Meridional Overturning Circulation.

The AC is an important agency which introduces IO water masses (for example, STSW) into the AR with  $\sigma_t$  less than  $27.5 \text{ kg}\cdot\text{m}^{-3}$  in the upper 1500 m. At greater depths, the water flowing within the AR circulation pattern consists primarily of Atlantic and CDW. The IO Water entering the AR is drawn from diverse sources: the thermocline of the South Indian Subtropical gyre, the thermocline water of the western tropical IO and within the lower thermocline, remnants of the high salinity-low

oxygen water from the Red Sea [48]. On entering the AR, the IO Water is altered by local air-sea interactions that cause a large turbulent heat loss from the surface, forming remnant winter mixed layers, marked by relatively high salinity and oxygen and by low salinity intrusions of South Atlantic Water.

Geostrophic transport computations reveal that the ACC flow by 23 Sv in 2009. The transport associated with the anticyclones which detach from the ARC varies between 3 to 9 Sv. Half of the ACC transport occurs in the 100 - 500 m layer. A comparison of water mass distribution for 2008 and 2009 reveals that MW distribution is restricted to 42.5°S and 41.9°S, while AASW extends to 57.6° and 46.6°S, respectively. In 2009, the along track HC and SC for the upper 750 m of the water column decreased each by 1% compared to those in 2008. Furthermore, HC and SC are lowered in the ACC domain by 36% and 40%, respectively. The HC and SC associated with ARF increases by 1% and 2%, respectively, in 2009 due to an increase in the transport of warm and saline water by 2%. However, at the merged SSTF + SAF1 + SAF2, the HC and SC dipped by 25% each, which is attributed to a very weak transport associated with those fronts in 2009.

In brief, the comparison of hydrographic data for two consecutive years yielded a wealth of information on the changes brought about by ACC circulation, air-sea interaction and AC system. It is noted that these results cannot be extrapolated to infer interannual variability. To highlight interannual variability we recommend that this region should be monitored over many years to capture signatures, especially those induced by warmer atmosphere/ocean in the climate change scenario.

#### 5. Acknowledgements

The QuikSCAT and AMSR-E data are produced by Remote Sensing Systems (<http://www.remss.com>) and sponsored by the NASA Earth Science *MEaSUREs DISCOVER* Project. The MADT data was downloaded from <http://www.avisioceanobs.com>. We acknowledge the Ministry of Earth Sciences for financing the XCTD probes. Dr. M. Nuncio was given the opportunity to participate and deploy XCTDs in 2009. This is NCAOR contribution No. 48/2012.

#### REFERENCES

- [1] L. Stramma, "The South Indian Ocean Current," *Journal of Physical Oceanography*, Vol. 22, No. 4, 1992, pp. 421-430.  
[doi:10.1175/1520-0485\(1992\)022<0421:TSIOC>2.0.CO;2](https://doi.org/10.1175/1520-0485(1992)022<0421:TSIOC>2.0.CO;2)
- [2] A. L. Gordon, "Indian-Atlantic Transfer of Thermohaline Water of the Agulhas Retroflexion," *Science*, Vol. 227,

- No. 4690, 1985, pp. 1030-1033.  
[doi:10.1126/science.227.4690.1030](https://doi.org/10.1126/science.227.4690.1030)
- [3] A. L. Gordon, "Interocean Exchange of Thermocline Water," *Journal of Geophysical Research*, Vol. 91, No. C4, 1986, pp. 5037-5046. [doi:10.1029/JC091iC04p05037](https://doi.org/10.1029/JC091iC04p05037)
- [4] W. P. M. de Ruijter, A. Biastoch, S. S. Drijfhout, J. R. E. Lutjeharms, R. P. Matano, T. Pichevin, P. J. van Leeuwen and W. Weijer, "Indian-Atlantic Interocean Exchange: Dynamics, Estimation and Impact," *Journal of Geophysical Research*, Vol. 104, No. C9, 1999, pp. 20885-20910. [doi:10.1029/1998JC900099](https://doi.org/10.1029/1998JC900099)
- [5] I. E. Robertson and A. J. Watson, "A Summertime Sink for Atmospheric Carbon Dioxide in the Southern Ocean between 80°W and 80°E," *Deep Sea Research-II*, Vol. 42, No. 4-5, 1995, pp. 1081-1091. [doi:10.1016/0967-0645\(95\)00067-Z](https://doi.org/10.1016/0967-0645(95)00067-Z)
- [6] M. Schröder and E. Fahrbach, "On the Structure and Transport of the Eastern Weddell Gyre," *Deep-Sea Research-II*, Vol. 46, No. 1-2, 1999, pp. 501-527. [doi:10.1016/S0967-0645\(98\)00112-X](https://doi.org/10.1016/S0967-0645(98)00112-X)
- [7] A. H. Orsi, W. D. Nowlin and T. Whitworth Jr., "On the Circulation and Stratification of the Weddell Gyre," *Deep-Sea Research-I*, Vol. 40, No. 1, 1993, pp. 169-203. [doi:10.1016/0967-0637\(93\)90060-G](https://doi.org/10.1016/0967-0637(93)90060-G)
- [8] W. J. Emery and J. Meincke, "Global Water Masses: Summary and Review," *Oceanologica Acta*, Vol. 9, 1986, pp. 383-391.
- [9] L. Stramma and J. R. E. Lutjeharms, "The Flow Field of the Subtropical Gyre of the South Indian Ocean," *Journal of Geophysical Research*, Vol. 102, No. C3, 1997, pp. 5513-5530. [doi:10.1029/96JC03455](https://doi.org/10.1029/96JC03455)
- [10] S. T. Gille, "Warming of the Southern Ocean since the 1950s," *Science*, Vol. 295, No. 5558, 2002, pp. 1275-1277. [doi:10.1126/science.1065863](https://doi.org/10.1126/science.1065863)
- [11] W. Cai, "Antarctic Ozone Depletion Causes an Intensification of the Southern Ocean Super-Gyre Circulation," *Geophysical Research Letters*, Vol. 33, No. 3, 2006. [doi:10.1029/2005GL024911](https://doi.org/10.1029/2005GL024911)
- [12] J. K. Willis, D. Roemmich and B. Cornuelle, "Combining Altimetric Height with Broadscale Profile Data to Estimate Steric Height, Heat Storage, Subsurface Temperature, and Sea-Surface Temperature Variability," *Journal of Geophysical Research*, Vol. 108, No. C9, 2003, p. 3292. [doi:10.1029/2002JC001755](https://doi.org/10.1029/2002JC001755)
- [13] Y.-H. Park, L. Gamberoni and E. Charriaud, "Frontal Structure, Water Masses, and Circulation in the Crozet Basin," *Journal of Geophysical Research*, Vol. 98, No. C7, 1993, pp. 12361-12385. [doi:10.1029/93JC00938](https://doi.org/10.1029/93JC00938)
- [14] I. M. Belkin and A. L. Gordon, "Southern Ocean Fronts from the Greenwich Meridian to Tasmania," *Journal of Geophysical Research*, Vol. 101, No. C2, 1996, pp. 3675-3696. [doi:10.1029/95JC02750](https://doi.org/10.1029/95JC02750)
- [15] M. D. Sparrow, K. J. Heywood, J. Brown and D. P. Stevens, "Current Structure of the South Indian Ocean," *Journal of Geophysical Research*, Vol. 101, No. C3, 1996, pp. 6377-6391. [doi:10.1029/95JC03750](https://doi.org/10.1029/95JC03750)
- [16] A. J. Luis and M. Sudhakar, "Upper-Ocean Hydrodynamics along Meridional Sections in the Southwest Indian Sector of the Southern Ocean during Austral Summer 2007," *Polar Science*, Vol. 3, No. 1, 2009, pp. 13-30. [doi:10.1016/j.polar.2009.03.001](https://doi.org/10.1016/j.polar.2009.03.001)
- [17] A. H. Orsi, T. Whitworth III and W. D. Nowlin Jr., "On the Meridional Extent and Fronts of the Antarctic Circumpolar Current," *Deep-Sea Research-I*, Vol. 42, No. 5, 1995, pp. 641-673. [doi:10.1016/0967-0637\(95\)00021-W](https://doi.org/10.1016/0967-0637(95)00021-W)
- [18] K. Mizuno and T. Watanabe, "Preliminary Results of *in-Situ* XCTD/CTD Comparison Test," *Journal of Oceanography*, Vol. 54, No. 4, 1998, pp. 373-380. [doi:10.1007/BF02742621](https://doi.org/10.1007/BF02742621)
- [19] S. Kizu, H. Onishi, T. Suga, K. Hanawa, T. Watanabe and H. Iwamiya, "Evaluation of the Fall Rates of the Present and Developmental XCTDs," *Deep-Sea Research-I*, Vol. 55, No. 4, 2008, pp. 571-586. [doi:10.1016/j.dsr.2007.12.011](https://doi.org/10.1016/j.dsr.2007.12.011)
- [20] R. Bailey, A. Gronell, H. Phillips, G. Meyers and E. Tanner, "CSIRO Cookbook for Quality Control of Expendable Bathythermograph (XBT) Data," *CSIRO Marine Laboratories Report 221*, CSIRO, Hobart, 1993.
- [21] X. Yuan, D. G. Martinson and Z. Dong, "Upper Ocean Thermohaline Structure and Its Temporal Variability in the Southeast Indian Ocean," *Deep-Sea Research-I: Oceanographic Research Papers*, Vol. 51, No. 2, 2003, pp. 333-347. [doi:10.1016/j.dsr.2003.10.005](https://doi.org/10.1016/j.dsr.2003.10.005)
- [22] Y.-H. Park, E. Charriaud and P. Craneguy, "Fronts, Transport, and Weddell Gyre at 30°E between Africa and Antarctica," *Journal of Geophysical Research*, Vol. 106, No. C2, 2001, pp. 2857-2879. [doi:10.1029/2000JC900087](https://doi.org/10.1029/2000JC900087)
- [23] A. G. Kostianoy, A. I. Ginzburg, M. Frankignoulle and B. Delille, "Fronts in the Southern Indian Ocean as inferred from Satellite Sea Surface Temperature Data," *Journal of Marine Systems*, Vol. 45, No. 1-2, 2004, pp. 55-73. [doi:10.1016/j.jmarsys.2003.09.004](https://doi.org/10.1016/j.jmarsys.2003.09.004)
- [24] <http://www.aviso.oceanobs.com>
- [25] N. Ducet, P.-Y. Le Traon and G. Reverdin, "Global High-Resolution Mapping of Ocean Circulation from TOPEX/Poseidon and ERS-1 and -2," *Journal of Geophysical Research*, Vol. 105, No. C8, 2000, pp. 19477-19498. [doi:10.1029/2000JC900063](https://doi.org/10.1029/2000JC900063)
- [26] M. Andres, J.-H. Park, M. Wimbush, X.-H. Zhu, K.-I. Chang and H. Ichikawa, "Study of the Kuroshio/Ryukyu Current System Based on Satellite-Altimeter and *in-Situ* Measurements," *Journal of Oceanography*, Vol. 64, No. 6, 2008, pp. 937-950. [doi:10.1007/s10872-008-0077-2](https://doi.org/10.1007/s10872-008-0077-2)
- [27] F. J. Wentz, C. L. Gentemann and P. D. Ashcroft, "On-Orbit Calibration of AMSR-E and the Retrieval of Ocean Products," *The 83rd AMS Annual Meeting*, Long Beach, 2003.
- [28] O. Boebel, J. R. E. Lutjeharms, C. Schmid, W. Zenk, T. Rossby and C. Barron, "The Cape Caudron: A Regime of Turbulent Inter-Ocean Exchange," *Deep-Sea Research II*, Vol. 50, No. 1, 2003, pp. 57-86. [doi:10.1016/S0967-0645\(02\)00379-X](https://doi.org/10.1016/S0967-0645(02)00379-X)
- [29] J. R. E. Lutjeharms and W. P. M. de Ruijter, "The Influence of the Agulhas Current on the Adjacent Coastal Ocean: Possible Impacts of Climate Change," *Journal of*

- Marine Systems*, Vol. 7, No. 2-4, 1996, pp. 321-336.  
[doi:10.1016/0924-7963\(95\)00010-0](https://doi.org/10.1016/0924-7963(95)00010-0)
- [30] W. P. M. de Ruijter, P. J. van Leeuwen and J. R. E. Lutjeharms, "Generation and Evolution of Natal Pulses: Solitary Meanders in the Agulhas Current," *Journal of Physical Oceanography*, Vol. 29, No. 12, 1999, pp. 3043-3055.  
[doi:10.1175/1520-0485\(1999\)029<3043:GAEONP>2.0.CO;2](https://doi.org/10.1175/1520-0485(1999)029<3043:GAEONP>2.0.CO;2)
- [31] M. Tsugawa and H. Hasumi, "Generation and Growth Mechanism of the Natal Pulse," *Journal of Physical Oceanography*, Vol. 40, No. 7, 2010, pp. 1597-1612.  
[doi:10.1175/2010JPO4347.1](https://doi.org/10.1175/2010JPO4347.1)
- [32] J. R. E. Lutjeharms, "The Role of Mesoscale Turbulence in the Agulhas Current System," *Elsevier Oceanography Series*, Vol. 50, 1989, pp. 357-372.  
[doi:10.1016/S0422-9894\(08\)70196-X](https://doi.org/10.1016/S0422-9894(08)70196-X)
- [33] C. D. Quartly and M. A. Srokosz, "Seasonal Variations in the Region of the Agulhas Retroflection: Studies with Geosat and FRAM," *Journal of Physical Oceanography*, Vol. 23, No. 9, 1993, pp. 2107-2124.  
[doi:10.1175/1520-0485\(1993\)023<2107:SVITRO>2.0.CO;2](https://doi.org/10.1175/1520-0485(1993)023<2107:SVITRO>2.0.CO;2)
- [34] C. J. Koblinsky, "The Global Distribution of  $f/H$  and the Barotropic Response of the Ocean," *Journal of Geophysical Research*, Vol. 95, No. C3, 1990, pp. 3213-3218.  
[doi:10.1029/JC095iC03p03213](https://doi.org/10.1029/JC095iC03p03213)
- [35] J. R. E. Lutjeharms and J. Cooper, "Interbasin Leakage through Agulhas Current Filaments," *Deep-Sea Research-I*, Vol. 43, No. 2, 1996, pp. 213-238.  
[doi:10.1016/0967-0637\(96\)00002-7](https://doi.org/10.1016/0967-0637(96)00002-7)
- [36] J. Ochoa and P. P. Niiler, "Vertical Vorticity Balance in Meanders Downstream the Agulhas Retroflection," *Journal of Physical Oceanography*, Vol. 37, No. 6, 2007, pp. 1740-1744.  
[doi:10.1175/JPO3064.1](https://doi.org/10.1175/JPO3064.1)
- [37] D. Stammer and C. Wunsch, "Temporal Changes in the Mesoscale Variability of the Oceans," *Deep-Sea Research-II*, Vol. 46, No. 1-2, 1999, pp. 77-108.  
[doi:10.1016/S0967-0645\(98\)00106-4](https://doi.org/10.1016/S0967-0645(98)00106-4)
- [38] N. Anilkumar, A. J. Luis, Y. K. Somayajulu, V. Ramesh Babu, M. K. Dash, S. M. Pednekar, K. N. Babu, M. Sudhakar and P. C. Pandey, "Fronts, Water Masses, and Heat Content Variability in the Western Indian Sector of the Southern Ocean during Austral Summer 2004," *Journal of Marine Systems*, Vol. 63, No. 1-3, 2006, pp. 20-34.  
[doi:10.1016/j.jmarsys.2006.04.009](https://doi.org/10.1016/j.jmarsys.2006.04.009)
- [39] Y.-H. Park, L. Gamberoni and E. Charriaud, "Frontal Structure, Water Masses, and Circulation in the Crozet Basin," *Journal of Geophysical Research*, Vol. 98, No. C7, 1993, pp. 12361-12385.  
[doi:10.1029/93JC00938](https://doi.org/10.1029/93JC00938)
- [40] Y.-H. Park and L. Gamberoni, "Large-Scale Circulation and Its Variability in the South Indian Ocean from TOPEX/POSEIDON Altimetry," *Journal of Geophysical Research*, Vol. 100, No. C12, 1995, pp. 24911-24929.  
[doi:10.1029/95JC01962](https://doi.org/10.1029/95JC01962)
- [41] Y.-H. Park, E. Charriaud and M. Fieux, "Thermohaline Structure of the Antarctic Surface Water/Winter Water in the Indian Sector of the Southern Ocean," *Journal of Marine Systems*, Vol. 17, No. 1-4, 1998, pp. 5-23.  
[doi:10.1016/S0924-7963\(98\)00026-8](https://doi.org/10.1016/S0924-7963(98)00026-8)
- [42] J. R. E. Lutjeharms, "Location of Frontal Systems between Africa and Antarctica: Some Preliminary Results," *Deep-Sea Research-I, Oceanography Research Papers*, Vol. 32, No. 12, 1985, pp. 1499-1509.  
[doi:10.1016/0198-0149\(85\)90100-1](https://doi.org/10.1016/0198-0149(85)90100-1)
- [43] J. F. Legeais, S. Speich, M. Arhan, I. J. Ansorge, E. Fahrbach, S. Garzoli and A. Klepikov, "The Baroclinic Transport of the Antarctic Circumpolar Current South of Africa," *Geophysical Research Letters*, Vol. 32, No. 24, 2005.  
[doi:10.1029/2005GL023271](https://doi.org/10.1029/2005GL023271)
- [44] S. R. Rintoul, S. Sokolov and J. Church, "A 6 Year Record of Baroclinic Transport Variability of the Antarctic Circumpolar Current at 140°E from Expendable Bathythermograph and Altimetry Measurements," *Journal of Geophysical Research*, Vol. 107, 2002, p. 3155.
- [45] P. L. Richardson, "Agulhas Leakage into the Atlantic Estimated with Subsurface Floats and Surface Drifters," *Deep-Sea Research-I*, Vol. 54, No. 8, 2007, pp. 1361-1389.  
[doi:10.1016/j.dsr.2007.04.010](https://doi.org/10.1016/j.dsr.2007.04.010)
- [46] M. Rouault, P. Penven and B. Pohl, "Warming in the Agulhas Current System since the 1980's," *Geophysical Research Letters*, Vol. 36, No. 12, 2009.  
[doi:10.1029/2009GL037987](https://doi.org/10.1029/2009GL037987)
- [47] D. Byrne, A. L. Gordon and W. Haxby, "Agulhas Eddies: A Synoptic View Using Geosat ERM Data," *Journal of Physical Oceanography*, Vol. 25, No. 5, 1995, pp. 902-917.  
[doi:10.1175/1520-0485\(1995\)025<0902:AEASVU>2.0.CO;2](https://doi.org/10.1175/1520-0485(1995)025<0902:AEASVU>2.0.CO;2)
- [48] A. L. Gordon, J. R. E. Lutjeharms and M. L. Gründlingh, "Stratification and Circulation at the Agulhas Retroflection," *Deep-Sea Research-I: Oceanographic Research Papers*, Vol. 34, No. 4, 1987, pp. 565-599.
- [49] J. R. E. Lutjeharms, "A Quantitative Assessment of Year-to-Year Variability in Water Movement in the Southwest Indian Ocean," *Nature*, Vol. 239, No. 91, 1972, pp. 59-60.
- [50] M. J. Orren, "Hydrology of the South West Indian Ocean," *Investigational Report of the Division for Sea Fisheries of South Africa*, Vol. 55, 1966, pp. 1-35.
- [51] H. R. Valentine, J. R. E. Lutjeharms and G. B. Brundrit, "The Water Masses and Volumetry of the Southern Agulhas Current Region," *Deep-Sea Research-I*, Vol. 40, No. 6, 1993, pp. 1285-1305.  
[doi:10.1016/0967-0637\(93\)90138-S](https://doi.org/10.1016/0967-0637(93)90138-S)
- [52] A. L. Gordon, "South Atlantic Thermohaline Ventilation," *Deep-Sea Research*, Vol. 28, No. 11, 1981, pp. 1239-1264.  
[doi:10.1016/0198-0149\(81\)90033-9](https://doi.org/10.1016/0198-0149(81)90033-9)
- [53] M. S. McCartney, "Subantarctic Mode Water," In: M. V. Angel, Ed., *A Voyage of Discovery*, Pergamon, New York, 1977.
- [54] M. S. McCartney, "The Subtropical Recirculation of Mode Waters," *Journal of Marine Research*, Vol. 40, 1982, pp. 427-464.
- [55] Y.-H. Park, L. Gamberoni and E. Charriaud, "Frontal Structure and Transport of the Antarctic Circumpolar Current in the South Indian Ocean Sector, 40°E-80°E," *Marine Chemistry*, Vol. 35, No. 1-4, 1991, pp. 45-62.

- [doi:10.1016/S0304-4203\(09\)90007-X](https://doi.org/10.1016/S0304-4203(09)90007-X)
- [56] A. P. S. Wong, N. L. Bindoff and A. Forbes, "Ocean-Ice Shelf Interaction and Possible Bottom Water Formation in Prydz Bay, Antarctica," In: S. S. Jacobs and R. F. Weiss, Eds., *Ocean, Ice and Atmosphere: Interactions at the Antarctic Continental Margin, Antarctic Research Series*, Vol. 75. AGU, Washington DC, 1998.
- [57] H. U. Sverdrup, M. W. Johnson and R. H. Fleming, "The Oceans: Their Physics, Chemistry, and General Biology," Prentice-Hall, Upper Saddle River, 1942.
- [58] K. Wyrski, "Oceanographic Atlas of the International Indian Ocean Expedition," National Science Foundation, Washington DC, 1971.
- [59] T. Whitworth III, A. H. Orsi, S. J. Kim, W. D. Nowlin Jr. and R. A. Locarnini, "Water Masses and Mixing Near the Antarctic Slope Front," In: S. S. Jacobs and R. F. Weiss, Eds., *Ocean, Ice and Atmosphere: Interactions at the Antarctic Continental Margin, Antarctic Research Series*, Vol. 75. AGU, Washington DC, 1998, pp. 1-27. [doi:10.1029/AR075p0001](https://doi.org/10.1029/AR075p0001)
- [60] E.-P. Lim and I. Simmonds, "Explosive Cyclone Development in the Southern Hemisphere and a Comparison with Northern Hemisphere Events," *Monthly Weather Review*, Vol. 130, No. 9, 2002, pp. 2188-2209.
- [doi:10.1175/1520-0493\(2002\)130<2188:ECDITS>2.0.CO;2](https://doi.org/10.1175/1520-0493(2002)130<2188:ECDITS>2.0.CO;2)
- [61] R. G. Peterson, W. D. Nowlin Jr. and T. Whitworth III, "Generation and Evolution of a Cyclonic Ring at Drake Passage in Early 1979," *Journal of Physical Oceanography*, Vol. 12, No. 7, 1984, pp. 712-719. [doi:10.1175/1520-0485\(1982\)012<0712:GAEOAC>2.0.CO;2](https://doi.org/10.1175/1520-0485(1982)012<0712:GAEOAC>2.0.CO;2)
- [62] O. Boebel, T. Rossby, J. R. E. Lutjeharms, W. Zenk and C. Barron, "Path and Variability of the Agulhas Return Current," *Deep-Sea Research II*, Vol. 50, No. 1, 2003, pp. 35-56. [doi:10.1016/S0967-0645\(02\)00377-6](https://doi.org/10.1016/S0967-0645(02)00377-6)
- [63] M. R. Jury, B. M. R. Pathack, C. J. D. W. Rautenbach and J. van Heerden, "Drought over South Africa and Indian Ocean SST: Statistical and GCM Results," *The Global Atmosphere and Ocean System*, Vol. 4, No. 1, 1996, pp. 47-63.
- [64] W. H. F. Smith and D. T. Sandwell, "Global Seafloor Topography from Satellite Altimetry and Ship Depth Soundings," *Science*, Vol. 277, No. 5334, 1997, pp. 1957-1962. [doi:10.1126/science.277.5334.1956](https://doi.org/10.1126/science.277.5334.1956)